

## Numerical analysis of a comprehensive model of M-phase control in *Xenopus* oocyte extracts and intact embryos

Bela Novak\* and John J. Tyson†

Department of Biology, Virginia Polytechnic Institute and State University, Blacksburg, Virginia 24060-0406, USA

\*Permanent address: Department of Agricultural Chemical Technology, Technical University of Budapest, 1521 Budapest Gellert Ter 4, Hungary  
†Author for correspondence

### SUMMARY

To contribute to a deeper understanding of M-phase control in eukaryotic cells, we have constructed a model based on the biochemistry of M-phase promoting factor (MPF) in *Xenopus* oocyte extracts, where there is evidence for two positive feedback loops (MPF stimulates its own production by activating Cdc25 and inhibiting Wee1) and a negative feedback loop (MPF stimulates its own destruction by indirectly activating the ubiquitin pathway that degrades its cyclin subunit). To uncover the full dynamical possibilities of the control system, we translate the regulatory network into a set of differential equations and study these equations by graphical techniques and computer simulation. The positive feedback loops in the model account for thresholds and time lags in cyclin-induced and MPF-induced activation of MPF, and the model can be fitted quantitatively to these experimental observations. The negative feedback loop is consistent with observed time lags in MPF-induced cyclin degradation. Furthermore, our model indicates

that there are two possible mechanisms for autonomous oscillations. One is driven by the positive feedback loops, resulting in phosphorylation and abrupt dephosphorylation of the Cdc2 subunit at an inhibitory tyrosine residue. These oscillations are typical of oocyte extracts. The other type is driven by the negative feedback loop, involving rapid cyclin turnover and negligible phosphorylation of the tyrosine residue of Cdc2. The early mitotic cycles of intact embryos exhibit such characteristics. In addition, by assuming that unreplicated DNA interferes with M-phase initiation by activating the phosphatases that oppose MPF in the positive feedback loops, we can simulate the effect of addition of sperm nuclei to oocyte extracts, and the lengthening of cycle times at the mid-blastula transition of intact embryos.

Key words: M-phase promoting factor, Cdc2-kinase, cyclin, Cdc25, Wee1, S-M coupling

### INTRODUCTION

Our present understanding of the molecular mechanism that controls entry into M phase has arisen primarily from genetic studies of yeast cells and biochemical studies of metazoan eggs and embryos (Nurse, 1990). For instance, MPF (M-phase promoting factor) was originally defined as an activity that induces maturation of frog primary oocytes, and it was subsequently found to appear transiently during both the meiotic divisions of oocytes and the mitotic divisions of fertilized eggs. Concurrently, a periodic protein, cyclin, was discovered in the early mitotic cycles of invertebrate embryos. As originally defined, MPF is a set of cytoplasmic factors, any one of which can induce oocyte maturation, but it has since come to be applied to one specific protein: the heterodimer of cyclin and Cdc2 (a protein kinase first identified in fission yeast).

Early embryonic division cycles have some unique and interesting properties: they are rapid and synchronous, they proceed in the absence of overall cell growth, and they can be dissociated from periodic DNA synthesis (Harvey, 1940;

Hara et al., 1980). Cell-free extracts of frog eggs, prepared by the methods of Hutchison et al. (1988) and Murray and Kirschner (1989), exhibit many of the same properties, such as periodic accumulation of cyclin, periodic activation of MPF, and the ability to cycle independently of DNA synthesis. Since a cell-free preparation is easier to manipulate and control than an intact egg, many molecular details about the activation of MPF and the coupling between DNA synthesis and mitosis have been derived from these extracts. The emerging picture is being used to understand the cell cycle of intact frog eggs and to generalize, as much as possible, to other eukaryotic cells.

We would like to contribute to this enterprise by introducing a practical theoretical approach to the study of M-phase control. By combining the results of many experimental studies of frog egg extracts, we construct a model of MPF activation that is biochemically sound but too complicated to understand by informal verbal reasoning. Therefore, we translate the model into precise mathematical equations and study its properties by accurate numerical simulation. The results are compared in quantitative detail

with experimental observations, to judge the credibility of the comprehensive model.

The molecular mechanism that controls entry into M phase is undeniably complex. The activity of MPF during the cell cycle is regulated in two different ways: by synthesis and degradation of cyclin, and by phosphorylation and dephosphorylation of Cdc2. Two major feedback signals govern the MPF regulatory system: (1) MPF modulates the kinases and phosphatases that determine its own activity, in a positive feedback loop; and (2) MPF stimulates the proteolytic machinery that degrades cyclin subunits and destroys MPF activity, thereby creating a negative feedback loop. Both of these signals operate with significant time delays that seem to have important physiological consequences. In addition, various 'checkpoint' controls impinge on the MPF network from outside (Murray, 1992).

After converting these ideas into mathematical equations, we shall, by computer simulations and graphical analysis, compare the model in detail with several important experimental studies: Solomon et al. (1990), on cyclin activation of MPF; Felix et al. (1990b), on MPF activation of cyclin degradation; Murray and Kirschner (1989), on MPF oscillations in oocyte extracts; Dasso and Newport (1990), on mitotic block by unreplicated DNA; Ferrell et al. (1991), on rapid MPF oscillations in intact embryos.

We hope to convince the reader that mathematical modeling of the MPF control system not only confirms accepted notions about how the system works but also gives new insights into the significance of thresholds, time lags, and the role of tyrosine phosphorylation in *Xenopus* oocyte extracts and intact embryos.

## A MODEL OF MPF ACTIVATION IN OOCYTE EXTRACTS

The fundamental components of M-phase control, which seem to be the same in all eukaryotic cells, are described in many excellent reviews: e.g. see Nurse (1990), Clarke and Karsenti (1991), Maller (1991), and Solomon (1993). M phase is triggered by a protein kinase, MPF, which is a heterodimer composed of a catalytic subunit (Cdc2 kinase) and a regulatory subunit (cyclin B). The level of Cdc2 protein remains constant throughout the cell cycle, whereas cyclin is periodically degraded. The activity of MPF is regulated by three important phosphorylation sites: an activating phosphorylation site at Thr161 and two inhibitory phosphorylation sites at Thr14 and Tyr15. In *Xenopus* the two inhibitory sites are dephosphorylated simultaneously, so it is sufficient to keep track only of the phosphorylation state of Tyr15. There are, therefore, four different phosphorylation states of the Cdc2-cyclin dimer (Fig. 1A). The four phosphorylation states are interconverted by kinases and phosphatases. In *Xenopus* extracts, Thr161 is phosphorylated by an enzyme called CAK ('Cdc2 activating kinase') and dephosphorylated by INH (an 'inhibitory' protein phosphatase of type 2A). The kinase and phosphatase that regulate the phosphorylation of Tyr15 are Wee1 and Cdc25, named after the genes *wee1* and *cdc25* that code for functionally homologous enzymes in fission yeast. The

active form of MPF is phosphorylated on Thr161 but not on Tyr15. Active MPF initiates M phase by phosphorylating a suite of target proteins involved in the major events of mitosis.

Cyclin binding facilitates the phosphorylations of Cdc2 (Solomon et al., 1992). Free Cdc2 monomers exist primarily in the dephosphorylated form, and newly synthesized cyclin subunits bind avidly to these monomers to form the unphosphorylated dimer. In extracts of *Xenopus* oocytes, unphosphorylated dimer is then quickly phosphorylated at Tyr15 and, to a great extent, at Thr161 as well. (The two sites can be phosphorylated in either order.) Thus, during interphase, MPF dimers accumulate in two inactive forms that are phosphorylated on Tyr15, the doubly phosphorylated form predominating (Solomon et al., 1992; Devault et al., 1992). The transition from interphase to mitosis is brought about by an abrupt dephosphorylation of these forms at Tyr15. In intact frog embryos, by contrast, tyrosine phosphorylation is not evident during the rapid mitotic cycles before the mid-blastula transition (Ferrell et al., 1991). A mechanism different from periodic phosphorylation of Tyr15 apparently drives these rapid cycles.

The activation of MPF in oocyte extracts, i.e. its conversion from the doubly phosphorylated form to the threonine-phosphorylated form, is abrupt because the kinase activity of Wee1 and the phosphatase activity of Cdc25 are dependent on MPF activity (see Fig. 1B): Wee1 is inhibited by active MPF, and Cdc25 is activated (Solomon et al., 1990). The activation of Cdc25 is accomplished by phosphorylation (Kumagai and Dunphy, 1992; Izumi et al., 1992), and Cdc25 is a substrate for cyclin B-Cdc2 kinase activity (Hoffmann et al., 1993; Izumi and Maller, personal communication). We assume that Wee1 is regulated similarly (Smythe and Newport, 1992; Devault et al., 1992; Coleman et al., 1993), for the following reason. If vanadate (which blocks Cdc25) is added to an M-phase extract (Solomon et al., 1990, Fig. 9), MPF loses activity only very slowly at first, presumably because Wee1 is kept inactive by MPF-dependent phosphorylation. It takes some time for the phosphatase that opposes MPF (step f in Fig. 1B) to activate Wee1, which then inactivates MPF. The long-recognized autocatalytic nature of MPF activation in oocytes (Masui and Markert, 1971; Gerhart et al., 1984) and in extracts (Cyert and Kirschner, 1988) is attributable to the feedback of MPF on Wee1 and Cdc25 activities (Murray, 1993). Only one such feedback is necessary for autocatalysis, but experiments suggest that two feedbacks are operative.

Cdc2-cyclin dimers are broken up by cyclin degradation (Murray et al., 1989). Cyclin is labelled for destruction by a ubiquitin-conjugating enzyme (Glotzer et al., 1991), and the activity of this enzyme (like Wee1 and Cdc25) is also regulated by MPF (Hunt, 1991). Activation of the cyclin-degradation pathway appears to be indirect because there is a significant time lag between a rise in MPF activity and subsequent degradation of cyclin (Felix et al., 1990b). This time lag has important dynamical consequences, as we shall see, so we introduce it into our model (Fig. 1B), following a suggestion by Hunt (1991), by placing an intermediary enzyme (IE) between MPF and the ubiquitin-conjugating enzyme (UbE). (Alternatively, the time lag could occur

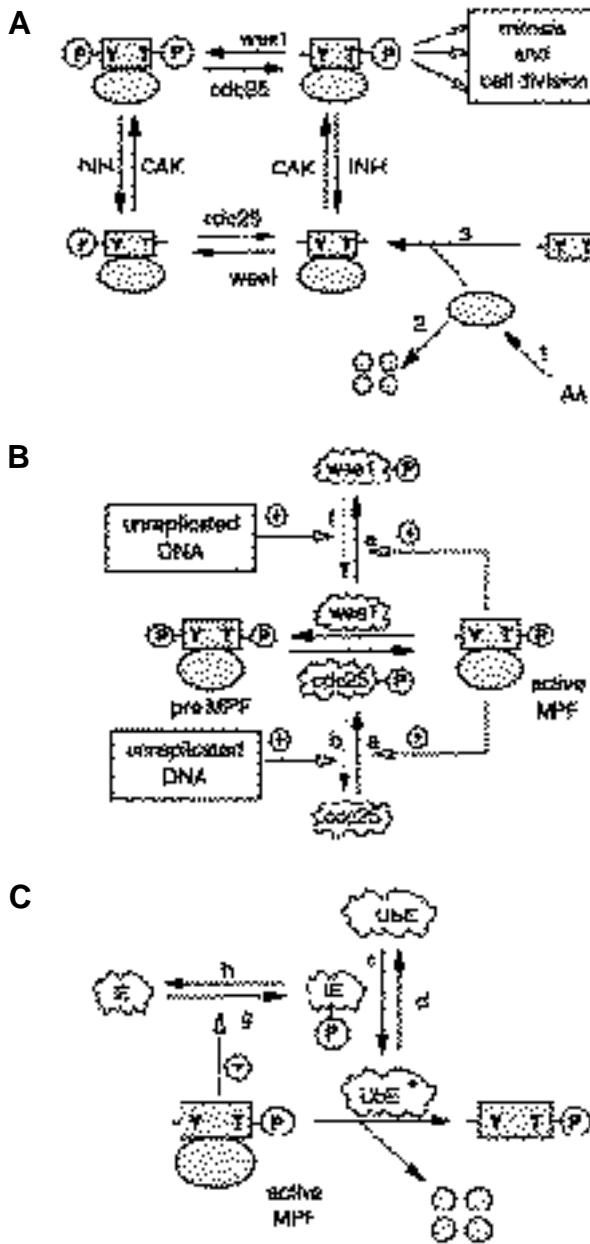


**Fig. 1.** The M-phase control system. (A) The phosphorylation states of MPF. Cyclin subunits (○), which are synthesized de novo from amino acids (step 1), bind with free Cdc2 (-□-) monomers (step 3) to form Cdc2-cyclin dimers. The dimer can exist in four different phosphorylation states (the dimer box) because of the action of two kinase-phosphatase pairs: Wee1/Cdc25, which acts at Tyr15 (Y), and CAK/INH, which acts at Thr161 (T). Active MPF, the dimer in the upper right-hand corner of the box, when in sufficient quantity, initiates mitosis by phosphorylating other proteins. All cyclin subunits (free or bound to Cdc2 in dimer complexes) are degraded by a ubiquitin pathway. (Step 2 indicates degradation of free cyclin; degradation of the dimers is left off the diagram to keep it simple.) (B) Positive feedback loops. Active MPF stimulates its own production from tyrosine-phosphorylated dimers by activating Cdc25 and inhibiting Wee1. We suspect that these signals are indirect, but intermediary enzymes are unknown and we ignore them in this paper. The signals from active MPF to Wee1 and Cdc25 generate an autocatalytic instability in the control system. We indicate also an 'external' signal from unreplicated DNA to Wee1 and Cdc25, which can be used to control the efficacy of the positive feedback loops. The letters a, b, e and f are used to label the rate constants for these reactions in Fig. 2. (C) Negative feedback loop. Active MPF stimulates its own destruction by indirectly activating the ubiquitin-conjugating enzyme (UbE) that labels cyclin subunits for destruction. The intermediary enzyme (IE) adds a delay to the signal, which makes this a potentially unstable negative feedback loop.

otic cells. The cell-cycle engine has some 'brakes' and 'accelerators' that convey external signals to the engine at specific 'checkpoints' in the cycle. For instance, incomplete DNA replication can block the cell cycle, whereas cell growth tends to speed it up. Evidence from *Xenopus* studies (Smythe and Newport, 1992; Izumi et al., 1992; Walker et al., 1992) suggests that unreplicated DNA exerts its decelerating effect by activating phosphatases b and f (Fig. 1B), which shift Cdc25 to its inactive form and Wee1 to its active form, consequently converting MPF to inactive, tyrosine-phosphorylated dimers.

To convert the regulatory system, shown diagrammatically in Fig. 1, into a set of mathematical equations, we assume that the chemical reactions take place in a more-or-less homogeneous chemical solution. Until more is known about the subcellular localization of components of the system, this is a reasonable place to start. Certainly we need to understand how the spatially homogeneous control system might behave before we can comprehend the unique features that may be introduced by compartmentalization of eukaryotic cells. Granted this starting point, the reaction rates are given by the law of mass action. For instance:

$$\begin{aligned} \left[ \frac{\text{time-rate-of-change}}{\text{of free cyclin conc}} \right] &= \left[ \frac{\text{rate of}}{\text{synthesis}} \right] \\ &- \left[ \frac{\text{rate of}}{\text{degradation}} \right] - \left[ \frac{\text{rate of association}}{\text{with Cdc2 monomers}} \right] \\ \frac{d}{dt} [\text{O}] &= k_1[\text{AA}] - k_2[\text{O}] - k_3[\text{O}][\square]. \end{aligned}$$

Similar equations can be written for Cdc2 monomer and the four dimers, as in Fig. 2. For the four regulatory

between ubiquitination of Cdc2-cyclin dimers and the proteolytic degradation of cyclin subunits. However, Glotzer et al. (1991) could detect only minor amounts of ubiquitinated cyclin. Since ubiquitinated forms are rapidly degraded, we put the time lag before the ubiquitination step.)

When MPF is activated, the ubiquitination system is turned on, and (we assume) all cyclin subunits (bound and free) are labelled and destroyed at the same rate. The phosphorylated Cdc2 monomers that are released are rapidly dephosphorylated (Lorca et al., 1992), so we only keep track of unphosphorylated Cdc2 monomer.

Fig. 1 summarizes our picture of the basic MPF control system, which Murray (1992) calls the cell-cycle engine. This network of reactions and feedback signals is firmly established for *Xenopus* eggs and extracts, and seems to apply in broad strokes to M-phase control in most eukary-

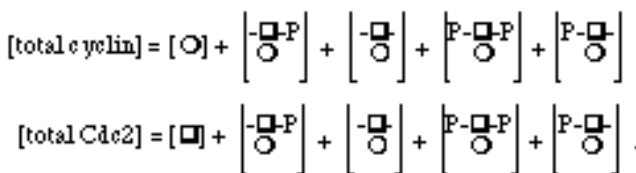
enzymes (Cdc25, Wee1, IE and UbE), we use Michaelis-Menten rate laws; for example:

$$\frac{d}{dt} [Cdc25-P] = \frac{k_a [\text{active MPF}] [Cdc25]}{K_a + [Cdc25]} - \frac{k_b [\text{PPase}] [Cdc25-P]}{K_b + [Cdc25-P]},$$

where  $[Cdc25-P]$  is the concentration of the more-active (phosphorylated) form of Cdc25 and  $[Cdc25]$  is the concentration of the less-active (unphosphorylated) form.\* We write  $[Cdc25]+[Cdc25-P]=[$ total Cdc25] and hold [total Cdc25] constant (Jessus and Beach, 1992). In Fig. 3A we illustrate how Wee1 and Cdc25 activities depend on MPF activity. The characteristic sigmoidal dependency is called zero-order ultrasensitivity by Goldbeter and Koshland (1981), who first described this effect.

The last three equations in Fig. 2 express the dependencies of the apparent first-order rate constants  $k_{25}$ ,  $k_{\text{wee}}$  and  $k_2$  on the concentrations of the less-active and more-active forms of the corresponding enzymes. The parameters  $V_i$  and  $V_i^*$  are turnover numbers for the less-active and more-active forms, respectively.

Let [total cyclin] and [total Cdc2] refer to the total concentrations of cyclin and Cdc2 subunits in monomeric and dimeric forms:



The time rate of change of [total cyclin] is obtained by adding together equations 1-5 of Fig. 2:

$$\frac{d}{dt} [\text{total cyclin}] = k_1 [\text{AA}] - k_2 [\text{total cyclin}].$$

Similarly, by adding equations 2-6, we find that:

$$\frac{d}{dt} [\text{total Cdc2}] = 0.$$

That is, [total Cdc2] does not change with time in our model, in agreement with experiments (e.g. see Ferrell et al., 1991, Fig. 4). For convenience, we express the concentrations of total cyclin and the Cdc2-cyclin dimers relative to the constant total concentration of Cdc2 subunits. In *Xenopus* egg extracts, this unit of concentration is approximately 100 nM (Solomon et al., 1990).

The model described in Figs 1 and 2 contains 31 parameters (18 rate constants and 13 characteristic concentra-

\*We use Michaelis-Menten kinetics for the activation and inhibition of the regulatory enzymes because this description introduces important nonlinearities into the mathematical equations. To justify this description we must assume that the substrates (Cdc25, etc.) are in great supply over the enzymes (the phosphatases and kinases) and that the effects of MPF on steps a, e and g in Fig. 1 are indirect (otherwise there would be complicated interference among these steps as the substrates compete with each other for the common kinase). These assumptions simplify the model considerably, but they could be relaxed if compelling experimental results call them into question.

$$\begin{aligned} &< \frac{\partial}{\partial t} [Cdc25] = V_1 k_{25} \cdot k_a [MPF] \cdot k_b [Cdc25-P] \\ &\leq \frac{\partial}{\partial t} [Cdc25-P] = k_{25} [Cdc25] - k_{25} k_a [MPF] \cdot k_b [Cdc25-P] + k_b [P-Cdc25] + k_2 [D-Cdc25] \\ &\geq \frac{\partial}{\partial t} [P-Cdc25] = k_{25} k_a [MPF] \cdot k_b [Cdc25-P] - k_{25} [Cdc25-P] + k_b [D-Cdc25] \\ &\leq \frac{\partial}{\partial t} [D-Cdc25] = k_{25} k_a [MPF] \cdot k_b [Cdc25-P] - k_{25} [Cdc25-P] + k_b [P-Cdc25] \\ &\geq \frac{\partial}{\partial t} [Wee1] = k_{wee} [Cdc25-P] \cdot k_{wee} + k_{wee} + k_{wee} [Cdc25-P] + k_{wee} [P-Wee1] \\ &\leq \frac{\partial}{\partial t} [P-Wee1] = k_{wee} [Cdc25-P] \cdot k_{wee} + k_{wee} [Cdc25-P] + k_{wee} [P-Wee1] \\ &\geq \frac{\partial}{\partial t} [IE] = \frac{k_2 (\text{active MPF}) \cdot (total Cdc25) \cdot (total cyclin) \cdot k_2 (P-Cdc25) \cdot k_2 (D-Cdc25)}{k_2 + (total Cdc25) \cdot (total cyclin) \cdot k_2 (P-Cdc25) \cdot k_2 (D-Cdc25)} \\ &\leq \frac{\partial}{\partial t} [P-IE] = \frac{k_2 (\text{active MPF}) \cdot (total Cdc25) \cdot (total cyclin) \cdot k_2 (P-Cdc25) \cdot k_2 (D-Cdc25)}{k_2 + (total Cdc25) \cdot (total cyclin) \cdot k_2 (P-Cdc25) \cdot k_2 (D-Cdc25)} \\ &\geq \frac{\partial}{\partial t} [UbE] = \frac{k_2 (\text{active MPF}) \cdot (total Cdc25) \cdot (total cyclin) \cdot k_2 (P-Cdc25) \cdot k_2 (D-Cdc25)}{k_2 + (total Cdc25) \cdot (total cyclin) \cdot k_2 (P-Cdc25) \cdot k_2 (D-Cdc25)} \\ &\leq \frac{\partial}{\partial t} [P-UbE] = \frac{k_2 (\text{active MPF}) \cdot (total Cdc25) \cdot (total cyclin) \cdot k_2 (P-Cdc25) \cdot k_2 (D-Cdc25)}{k_2 + (total Cdc25) \cdot (total cyclin) \cdot k_2 (P-Cdc25) \cdot k_2 (D-Cdc25)} \\ &\geq k_{25} = V_{25} \cdot (total Cdc25) \cdot (total cyclin) \cdot V_{25} \cdot [Cdc25-P] \\ &\leq k_{wee} = V_{wee} \cdot (total Cdc25) \cdot (total cyclin) \cdot V_{wee} \cdot (total Wee1) \cdot (total Cdc25-P) \\ &\geq k_2 = V_2 \cdot (total Cdc25) \cdot (total cyclin) \cdot V_2 \cdot [Cdc25-P] \end{aligned}$$

**Fig. 2.** The mathematical model. The ten differential equations are derived from the reaction mechanism in Fig. 1: the first six follow mass-action kinetics and the next four follow Michaelis-Menten kinetics. The total concentrations of the enzymes Cdc25, Wee1, IE and UbE (active+inactive forms) are assumed to be constant. The rate constants  $k_{25}$ ,  $k_{\text{wee}}$  and  $k_2$  that appear in equations 1-6, are defined by equations 11-13, in terms of the concentrations of the alternative forms of Cdc25, Wee1 and UbE.

tions) that need to be specified before the differential equations can be solved. We specify a basal set of rate parameters in Table 1.

Because [total Cdc2]=constant, there are only nine independent differential equations in Fig. 2. The behavior of our model of the cell-cycle engine is completely determined by these equations. Our job is to find solutions that conform with experimentally observed behavior of the MPF control system in *Xenopus* embryos and extracts.

All of the results to follow were derived by numerical solution of the differential equations in Fig. 2, using the parameter values in Table 1 or slight modifications thereof. The equations were solved on an IBM PC using the software PhasePlane (Ermentrout, 1990) and Time-Zero (Kirchner, 1990). We used Gear's method (with tolerance= $10^{-4}$ ) because it is the best method for solving systems of nonlinear ordinary differential equations with rate constants that differ by several orders of magnitude (Table 1).

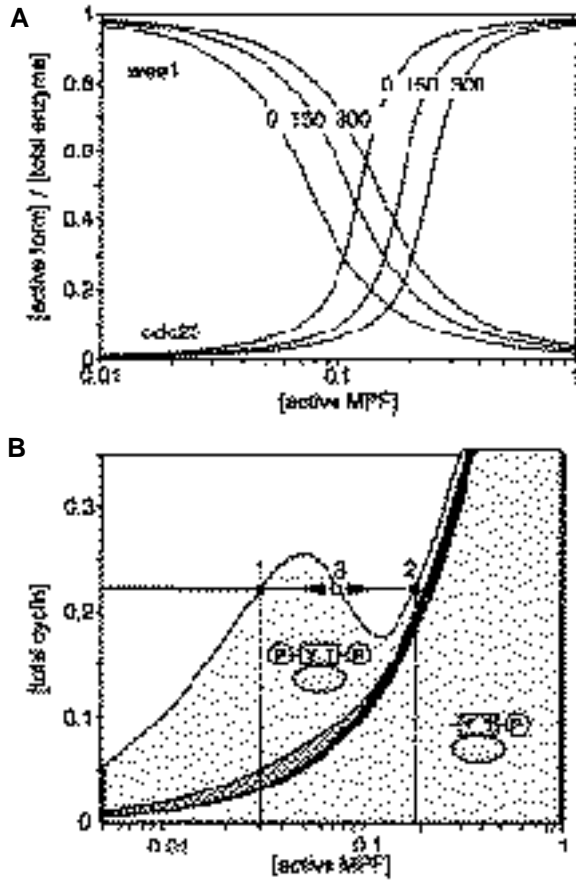


**Fig. 3.** Positive feedback and the N-shaped dimer equilibrium curve. (A) Dynamics of the tyrosine-modifying enzymes. The curve labelled Wee1 is the steady-state fraction of Wee1 in the active form as a function of [active MPF], obtained by solving equation 8 of Fig. 2. Similarly, Cdc25 is obtained from equation 7. The curves are shifted to the right in the presence of unreplicated DNA (0, 150, and 300 nuclei/μl extract), which increases the activities of phosphatases b and f. Parameter values as in Table 1, except: for 150 nuclei/μl,  $k_b=0.1836$  and  $k_f=0.1468$ , and for 300 nuclei/μl,  $k_b=0.2422$  and  $k_f=0.1937$ . (B) Equilibrium curves for the dimer box. The lowest curve represents the amount of cyclin contributed by active MPF; it is given by the equation [total cyclin]=[active MPF], and appears to rise exponentially because the abscissa is plotted on a log scale. The next curve up is [total cyclin]=[active MPF]+[unphosphorylated dimer]=[active MPF](1+ $k_{INH}/k_{CAK}$ ). The third curve from the bottom adds to the second the concentration of the Tyr15-phosphorylated dimer, and the top curve is the sum of the concentrations of all four forms. Parameter values are given in Table 1. Concentrations on the ordinate and abscissa are both scaled with respect to the constant total concentration of Cdc2 protein. Thus, [total cyclin]=1 means there are equal numbers of cyclin and Cdc2 subunits, and [active MPF]=1 means all Cdc2 subunits are associated with cyclin and phosphorylated on Thr161 only.

## THE EQUILIBRIUM DISTRIBUTION OF DIMERS

To understand how this system works, consider first the interconversion of the four dimer forms. If we add to a solution of Cdc2 monomers a fixed amount of nondegradable cyclin, how will the resulting dimers be distributed among

**Table 1. Basal set of parameters for the mathematical model in Fig. 1**

The following parameters are dimensionless:

$K_a / [\text{total Cdc25}] = 0.1$	$K_b / [\text{total Cdc25}] = 0.1$
$K_c / [\text{total UbE}] = 0.01$	$K_d / [\text{total UbE}] = 0.01$
$K_e / [\text{total Wee1}] = 0.3$	$K_f / [\text{total Wee1}] = 0.3$
$K_g / [\text{total IE}] = 0.01$	$K_h / [\text{total IE}] = 0.01$

The following parameters have units ( $\text{min}^{-1}$ ):

$k_1 [\text{AA}] / [\text{total Cdc2}] = 0.01 (0.018)$	$k_3 [\text{total Cdc2}] = 1.0$
$V_2 [\text{total UbE}] = 0.015 (0.03)$	$V_2 [\text{total UbE}] = 1.0 (1.25)$
$V_{25} [\text{total Cdc25}] = 0.1$	$V_{25} [\text{total Cdc25}] = 2.0$
$V_{wee} [\text{total Wee1}] = 0.1$	$V_{wee} [\text{total Wee1}] = 1.0$
$k_{CAK} = 0.25$	$k_{INH} = 0.025$
$k_a [\text{total Cdc2}] / [\text{total Cdc25}] = 1.0 (0.5)$	$k_b [\text{PPase}] / [\text{total Cdc25}] = 0.125 (0.0375)$
$k_c [\text{total IE}] / [\text{total UbE}] = 0.1 (0.4)$	$k_d [\text{antiIE}] / [\text{total UbE}] = 0.095 (0.25)$
$k_e [\text{total Cdc2}] / [\text{total Wee1}] = 1.33 (0.67)$	$k_f [\text{PPase}] / [\text{total Wee1}] = 0.1 (0.05)$
$k_g [\text{total Cdc2}] / [\text{total IE}] = 0.65 (2.0)$	$k_h [\text{PPase}] / [\text{total IE}] = 0.087 (0.27)$

The basal parameter set was used for simulations of oocyte extracts. The alternative values (in parentheses) were used to simulate the intact embryo.

the four phosphorylation states? Exactly this experiment was carried out by Solomon et al. (1990): to egg extracts they added recombinant cyclin (GT cyclin) whose modified N terminus renders it nondegradable by the ubiquitin pathway, and they also added cycloheximide to block cyclin synthesis from maternal mRNA. They then assayed Cdc2-kinase activity as a function of time and amount of GT cyclin added.

Since cyclin subunits bind quickly and nearly irreversibly to Cdc2 (Solomon et al., 1990), we can describe the equilibrium distribution of dimers by the equation:

$$\begin{aligned} [\text{total cyclin}] &= \left[ \frac{-\square-P}{O} \right] + \left[ \frac{-\square}{O} \right] + \left[ \frac{P-\square-P}{O} \right] + \left[ \frac{P-\square}{O} \right] \\ &= \left[ \frac{-\square-P}{O} \right] + \frac{k_{INH}}{k_{CAK}} \left[ \frac{-\square-P}{O} \right] + \frac{k_{wee}}{k_{25}} \left[ \frac{-\square-P}{O} \right] + \frac{k_{INH}k_{wee}}{k_{CAK}k_{25}} \left[ \frac{-\square-P}{O} \right] \\ &= [\text{active MPF}] \left( 1 + \frac{k_{INH}}{k_{CAK}} \right) \left( 1 + \frac{k_{wee}}{k_{25}} \right). \end{aligned}$$

In Fig. 3B we plot [total cyclin] against [active MPF], as predicted by this equation. The curve has a 'serpentine' shape because  $k_{wee}$  and  $k_{25}$  are not constants but functions of [active MPF], as shown in Fig. 3A.

The curves in Fig. 3B describe the equilibrium distribution of cyclin among various dimer forms as a function of [active MPF]. The bottom curve shows the amount of cyclin sequestered in active MPF dimer; the shaded area above it, the contribution by the unphosphorylated dimer; the hatched area, the contribution by the Tyr15-phosphorylated dimer; and the stippled area on top, the contribution by the doubly phosphorylated dimer. For a given total cyclin concentration, one can read directly from the graph the amount of cyclin in each dimer group at equilibrium.

For instance, at point 1, where [total cyclin]=0.225 (in units of total Cdc2), the dimers are about 78% doubly phosphorylated and 8% tyrosine-phosphorylated, with only about 13% active MPF and 1% unphosphorylated dimer. In these calculations we have chosen  $k_{CAK}/k_{INH}=10$  to conform with the experimental finding that inactive MPF exists primarily as the doubly phosphorylated form (Solomon et al., 1990; Devault et al., 1992). In what follows, we shall refer to the uppermost curve in Fig. 3B as the 'dimer equilibrium curve', with the understanding that, to reconstruct the equilibrium distribution of all four dimer forms, one must employ the full set of curves in Fig. 3B.

Because active MPF activates Cdc25 and inhibits Wee1, the equilibrium curve is N-shaped and, at intermediate levels of cyclin, there are two alternative states of dimer equilibrium: a state of low MPF activity (point 1), where most dimers are phosphorylated on Tyr15, and a state of high activity (point 2), where most dimers have been converted to active MPF. There is a third state of intermediate MPF activity (point 3), but this state is unstable and therefore unreachable.

## THRESHOLDS AND LAGS

To simulate the experiments of Solomon et al. (1990), described at the beginning of the previous section, we solve the equations in Fig. 2 given the parameter values in Table 1, except  $k_1=0$  (no cyclin synthesis) and  $V_2=V_2=0$  (no cyclin degradation). In Fig. 4A we plot [active MPF] as a function of time for simulations starting with different initial values of [total cyclin]. For small amounts of added cyclin (25% or less of the total Cdc2 in the mix), the extract generates very little MPF activity, but larger amounts (40% or more) induce considerable activation of MPF. By referring to the inset of Fig. 4A, we see that the threshold for cyclin-induced activation of MPF lies somewhere between 25 and 30%. Increasing the amount of cyclin added increases the final level of MPF activity and the time lag drops quickly to a minimum delay of about 8 minutes. (Following Solomon et al. (1990), we define lag to be the time necessary for MPF activity to reach 50% of its final value.) During the lag period, Cdc2-cyclin dimers are transiently phosphorylated on Tyr15.

The cyclin threshold is a reflection of the serpentine shape of the dimer equilibrium curve, as we now explain. Since the extract is prepared with cycloheximide to block endogenous cyclin synthesis, only unphosphorylated Cdc2 monomers are present initially. When GT cyclin is added, unphosphorylated dimers are formed and begin to be phosphorylated. As indicated in Fig. 4B, the state of the system, specified by the coordinates [active MPF] and [total cyclin], will move along a horizontal line (because GT cyclin is nondegradable and its total concentration remains constant) until it reaches the nearest branch of the dimer equilibrium curve, at which point the four dimers will be distributed according to the set of curves in Fig. 3B. As shown in Fig. 4B, for values of [total cyclin] below 0.26, the control system stops on the branch of equilibrium states of low MPF activity, and a slight increase in cyclin level results in only a small increase in MPF activity. However, when

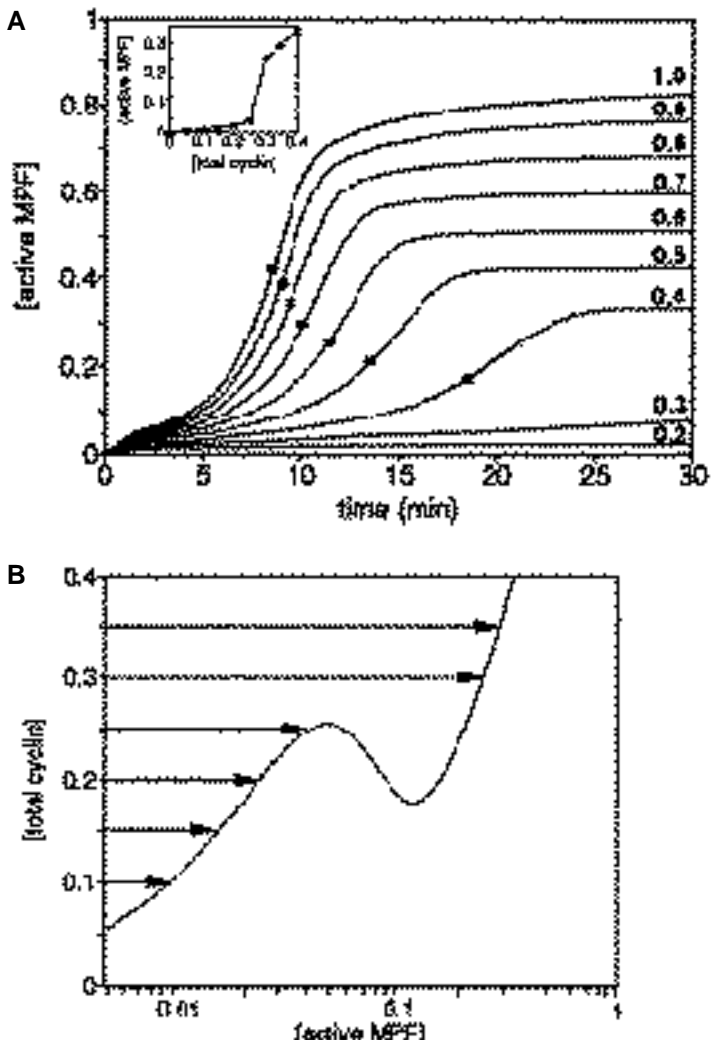


**Fig. 4.** Cyclin-induced activation of MPF. (A) Threshold and lag. The equations in Fig. 2 were solved using the parameter values in Table 1, except  $k_1=V_2=V_2=0$ . Initial conditions: all Cdc2 as unphosphorylated monomer, Wee1 in the active form and Cdc25 in the inactive form (because [active MPF]=0 initially), and cyclin monomers added at different levels relative to [total Cdc2]. We plot [active MPF] as a function of time. The numbers on each curve give the total amount of cyclin added to each extract. Compare these curves to those of Clarke et al. (1992), Fig. 1A, and of Solomon et al. (1990), Fig. 3. The black squares mark the lag point, at 50% of final MPF activity. As [total cyclin] increases, lag time decreases and eventually levels off at about 8 minutes, which is considerably shorter than the 20 minute lags observed by Solomon et al. (1990). But they ran their experiments at 15°C in order to lengthen the lag time (to make it easier to measure), whereas our parameter set (Table 1) has been adjusted to model extracts at 23°C. In the inset we plot final MPF activity as a function of cyclin level, for comparison with Solomon et al. (1990), Fig. 4B. (B) The N-shaped equilibrium curve implies a cyclin threshold. As [total cyclin] in the extract is increased, there is an abrupt threshold for activation of MPF, given by the local maximum of the dimer equilibrium curve. The arrows indicate that, above the equilibrium curve, [active MPF] is an increasing function of time. Below the curve, [active MPF] is a decreasing function of time.

[total cyclin] is increased above the local maximum of the equilibrium curve, MPF activity increases sharply as dimers are converted almost completely into active MPF - hence the phenomenon of a cyclin threshold for MPF activation.

The lag time, which is explicitly expressed in Fig. 4A, is implicit in Fig. 4B: one must imagine the state of the system moving along the horizontal line, at variable speed, from zero active MPF to the equilibrium curve. For instance, at [total cyclin]=0.3 in Fig. 4B, as [active MPF] increases, the system passes just above the dimer equilibrium curve, and, as it does so, the velocity of its motion becomes very slow because the equilibrium curve is a locus of states for which the net rate of dimer transformations is identically zero. Nonetheless, the system eventually escapes the stagnation zone near the equilibrium curve, accelerates as the positive feedback loops engage, and moves to the equilibrium state of high MPF activity. Indeed, from our simulations, the lag time increases in inverse proportion to the distance between the (fixed) cyclin level and the maximum of the dimer equilibrium curve (the threshold):

$$\text{lag} = (\text{min lag}) \frac{[\text{total cyclin}]}{[\text{total cyclin}] - \text{threshold}} .$$

For instance, for the parameter values in Table 1, min lag=6.4 min and threshold=0.26.

The long lag time for cyclin levels close to threshold may engender two misinterpretations of experimental data. First, the cyclin threshold will always be overestimated, because we assay MPF activity after only a limited period of time has elapsed. If we were to wait longer, we could always find lower cyclin levels that would induce MPF activation eventually. This effect is illustrated in Fig. 4A, where [total cyclin]=0.3 induces MPF activation with a time lag longer than 30 minutes. Second, this very observation might suggest that, if we waited long enough, *any* amount of cyclin, no matter how small, will induce some MPF activation, i.e. there is no such thing as a cyclin threshold, only a cyclin-dependent lag time. This conclusion would be incorrect because, if our picture of a serpentine equilibrium curve is true, there must always be a discontinuous jump in final MPF activity as a function of initial cyclin level, and this jump defines the cyclin threshold.

In Fig. 5 we illustrate the effects of various biochemical agents on the cyclin threshold and lag period. For instance, supplementation of oocyte extracts with exogenous INH causes both the cyclin threshold and the lag time to increase (Solomon et al., 1990, Fig. 4A,D). We can simulate these results provided that INH catalyses both Thr161 dephosphorylation (step INH in Fig. 1A) and Cdc25 dephosphorylation (step b in Fig. 1B), as suggested by Clarke et al. (1993) and Murray (1993). Conversely, okadaic acid, an inhibitor of type 1 and 2A phosphatases at the concentration used, abolishes the cyclin threshold because it inhibits phosphatases b and f, which are essential for operation of the positive feedback loops. Unreplicated DNA increases the threshold by increasing the activities of phosphatases b and f, and this effect can be counteracted by increasing levels of Cdc25. These effects and others are summarized in Table 2. In all cases the model is in qualitative agreement with experimental observations.

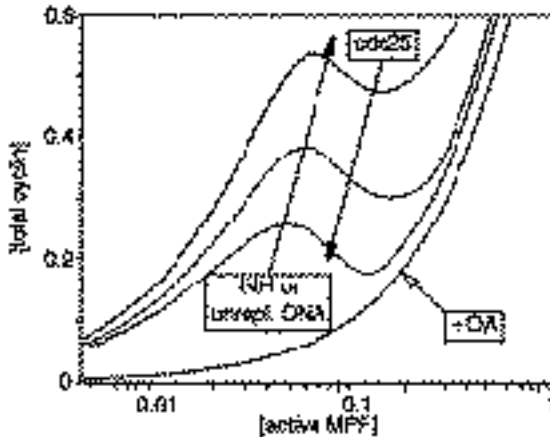


**Fig. 5.** Modulating the cyclin threshold. Increasing levels of INH or unreplicated DNA cause an increase in the cyclin threshold, whereas increasing levels of Cdc25 cause a decrease, and large doses of okadaic acid eliminate the cyclin threshold (compare with Solomon et al. (1990), Fig. 4B and D).

**Table 2. Factors effecting cyclin threshold and lag**

Treatment	Parameter change	Predicted effect		Observed effect	
		Threshold and Lag	Threshold	Lag	ND
+ INH (1)	$k_{\text{INH}}, k_b$				
+ CAK	$k_{\text{CAK}}$				
+ Okadaic acid*	$k_b = k_f = k_{\text{INH}} = 0$		0,	0	ND
+ Vanadate*	$V_{25}, V_{25}$				ND
+ Cdc25†‡	[total Cdc25]				ND
+ Wee1	[total Wee1]				ND
+ unrep DNA§	$k_b, k_f$				ND

\*Solomon et al. (1990)  
†Gautier et al. (1991)  
‡Hoffmann et al. (1993)  
§Dasso and Newport (1990)  
0, abolished; ND, not determined

Our picture of cyclin thresholds and lags can be tested by two types of experiments. First of all, the N-shaped dimer equilibrium curve suggests that there is not only a cyclin threshold for MPF activation (the local maximum of the curve) but also a cyclin threshold for MPF inactivation (the local minimum of the curve). That is, if we decrease the amount of cyclin in an extract prepared in a state of high MPF activity, we should observe a threshold cyclin level below which MPF is abruptly inactivated by tyrosine phosphorylation (Novak and Tyson, 1993). Secondly, our model predicts a hyperbolic relation between lag time and cyclin level, which contradicts the observations of Solomon et al. (1990) and Clarke et al. (1992). We suspect that in these experiments  $[\text{total cyclin}] \gg \text{threshold}$ , so the lag time is approximately equal to the minimum lag in all their measurements. Accurate measurements of lag time at cyclin levels closer to threshold should reveal the hyperbolic relation. The cyclin threshold and minimum lag are most accurately determined from such data by a double-reciprocal plot of  $1/\text{lag}$  versus  $1/[\text{cyclin}]$ .

In addition to cyclin thresholds, there is also an MPF threshold for MPF activation (Fig. 3B). Choose a cyclin

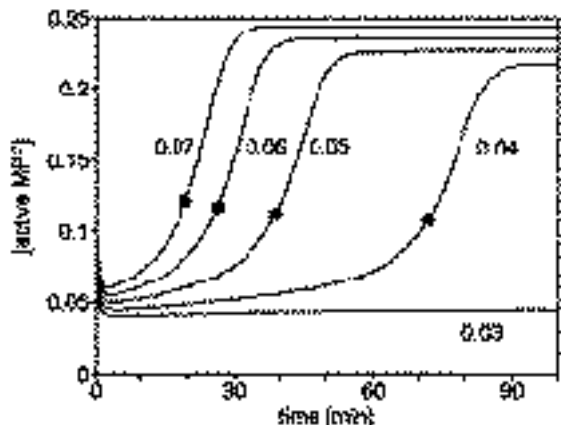


**Fig. 6.** Threshold and time lag in MPF-induced activation of MPF. For a fixed cyclin level of 0.225, we add increasing amounts of exogenous active MPF (0.03 to 0.07). Compare with Cyert and Kirschner (1988), Fig. 2. For subthreshold additions (e.g. 0.03) MPF activity returns quickly to the stable dimer equilibrium shown on the left of Fig. 3B, whereas suprathreshold additions induce a transition to the dimer equilibrium state of high MPF activity. During the transition the system is more-or-less slowly departing from the intermediate branch of unstable dimer equilibrium states. The lag period, the time necessary to achieve half-maximal MPF activity (black circles), is very long at first but decreases rapidly as more MPF is added.

level just below threshold and let the extract come to equilibrium at low MPF activity ( $G_2$  arrest: point 1 in Fig. 3B). If a small amount of exogenous active MPF is added to the extract, the regulatory system will recover to the stable state of low MPF activity. But if a sufficient amount of active MPF is added (beyond point 3), the positive feedback loops will be switched on and MPF activity will increase to even higher levels (point 2) as the endogenous stores of inactive dimers become tyrosine-dephosphorylated. Thus, for subthreshold cyclin levels, there is an MPF threshold for excitation of the control system (Fig. 6). This threshold is a major characteristic of classical MPF assays by microinjection into  $G_2$ -arrested primary oocytes (Wu and Gerhart, 1980, Fig. 2; Miake-Lye et al., 1983, Fig. 6, open circles) or into  $G_2$ -arrested extracts (Dunphy and Newport, 1988, Fig. 2). There is also a lag time associated with MPF-dependent MPF activation; a lag that can be very long for MPF perturbations just above threshold (Fig. 6).

## CYCLIN DEGRADATION

The previous section was based on an experimental protocol in which nondegradable cyclin is added to extracts blocked from protein synthesis by cycloheximide. The next step towards a more realistic situation is to follow the loss of degradable cyclin in extracts supplemented with exogenous MPF, in the presence of cycloheximide to prevent new cyclin synthesis (Felix et al., 1990b). For small amounts of added MPF, cyclin is very stable in these interphase extracts. However, when Felix et al. added active MPF at or above the level characteristic of mitotic oocytes, both cyclin (see their Fig. 1A) and MPF activity (their Fig.

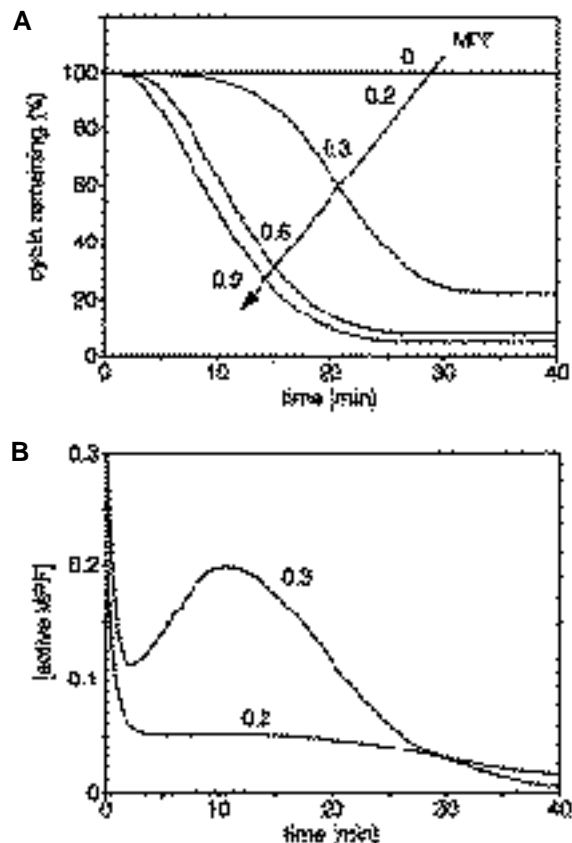


**Fig. 7.** MPF activation of cyclin degradation. The M-phase control system is initially prepared in an equilibrium state of low MPF activity, with no cyclin synthesis ( $k_1=0$ ). Cyclin is slowly degraded because UbE is predominantly in the less-active form. The system is perturbed by addition of active MPF in varying amounts (0.2... 0.9), and we follow cyclin degradation (A) and MPF activity (B) as functions of time. The amount of cyclin remaining is always expressed as a fraction of the amount remaining in the control preparation (0) to which no active MPF is added. Compare (A) with Felix et al. (1990b), Fig. 1A. Compare (B) with Felix et al. (1990b), Fig. 2B (panel 2).

2B) disappeared rapidly after a significant time delay. Fig. 7A shows a simulation of this experiment. Notice that an MPF level of 0.2 does not initiate cyclin degradation but a level of 0.3 does, after a 15–20 minute lag. Adding more MPF shortens the lag but leaves the maximum rate of cyclin degradation almost unchanged.

It is difficult to predict by casual verbal arguments the precise outcome of this type of experiment because MPF activation of cyclin degradation is fraught with conflicting molecular signals. In the original interphase extract, MPF activity is low (because cyclin level is below threshold and dimers are mostly tyrosine-phosphorylated), and the cyclin degradation machinery is only slightly engaged. What happens after addition of exogenous active MPF? Since Wee1 activity is large and Cdc25 activity is small in the interphase extract, active MPF will begin to be inactivated by tyrosine phosphorylation. But, at the same time, active MPF will start inactivating Wee1 and activating Cdc25, which may eventually lead to activation of tyrosine-phosphorylated dimers. Which of these opposing processes wins? Fur-

thermore, exogenous active MPF also stimulates the ubiquitin pathway which, after a time lag, begins to degrade all cyclin subunits in the extract. Of course, as MPF activity comes down, the cyclin degradation machinery turns off again at some point. In Fig. 7B we show the time course of MPF activity in this type of experiment as predicted by our model. For small additions of MPF ( $< 0.2$ ), MPF activity drops quickly at first, as MPF is inactivated by Wee1, and then slowly as all dimers are broken up by slow cyclin degradation. For larger additions ( $> 0.3$ ), MPF activity first drops (tyrosine phosphorylation), then rises (tyrosine dephosphorylation), then drops again (fast cyclin degradation).

### AUTONOMOUS OSCILLATIONS IN OOCYTE EXTRACTS

In *Xenopus* eggs and extracts under natural conditions, both MPF activity and total cyclin level will fluctuate according to the rate laws that specify the time-rate-of-change of the cell-cycle engine. According to our model, the state of the cell cycle engine can be represented by a point in a nine-dimensional space of state-variables (four dimers, four regulatory enzymes, and total cyclin), and this point is driven through state space by the rate laws of the engine (the differential equations in Fig. 2). This image is hard to visualize, to say the least, but much useful information can be derived from a two-dimensional projection of the nine-dimensional state space, in the same way that we find photographs to be useful representations of real three-dimensional objects. The two dimensions that we choose are active MPF and total cyclin, and we approximate the state of the full dynamical system by a point on the plane spanned by [active MPF] and [total cyclin]. Following standard mathematical terminology, we call this plane the 'phase plane.' As the state of the cell-cycle engine changes with time, the state-point moves around on the phase plane, as if driven by some underlying force field.

The force field is determined in large measure by two characteristic curves. The dimer equilibrium curve we have already described (Fig. 4B): if the instantaneous state of the system does not lie on the dimer equilibrium curve, then [active MPF] will change in time to bring the dimer distribution closer to equilibrium. The second curve, which we call the cyclin balance curve, is determined by equating the rate of cyclin synthesis to the rate of cyclin degradation. If the state is displaced from this curve, then [total cyclin] will adjust in the direction that equalizes the rates of cyclin synthesis and degradation. Since:

$$\frac{d}{dt} [\text{total cyclin}] = k_1 [\text{AA}] - k_2 [\text{total cyclin}],$$

the cyclin balance curve is given by  $k_1 [\text{AA}] = k_2 [\text{total cyclin}]$ , or

$$[\text{total cyclin}] = k_1 [\text{AA}] / k_2,$$

where  $k_2$  is a function of [active MPF]. If the cyclin degradation machinery is in equilibrium, we can calculate  $k_2$  as a function of [active MPF] from equations 9, 10 and 13 of Fig. 2.

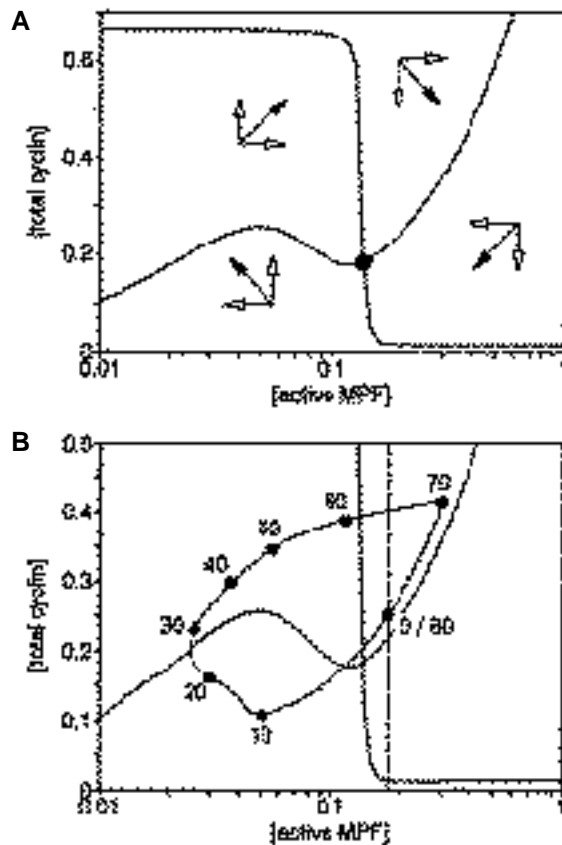


**Fig. 8.** Oscillatory dynamics of the M-phase control system. (A) Dynamical portrait. The cyclin balance curve (the sigmoidal curve) and the dimer equilibrium curve (the N-shaped curve) are plotted together on the phase plane. The arrows indicate the directions in which [total cyclin] and [active MPF] are changing (see text). (B) Limit cycle oscillations. Numerical solution of the differential equations in Fig. 2, with basal parameter values in Table 1, is projected onto the phase plane. The closed orbit, called a 'limit cycle', corresponds to sustained oscillations in [active MPF], [total cyclin], and the other seven variables of the system, with a period of 80 minutes. The numbers along the limit cycle represent time (in minutes) after exit from mitosis. Notice that there are places where the state-point is moving in the 'wrong' direction, according to the arrows in Fig. 8A, because the direction field predicted by the dimer equilibrium and cyclin balance curves is not exactly correct for the full nine-dimensional dynamical system.

In Fig. 8A the cyclin balance curve is plotted on the phase plane. It is a sigmoidal curve because  $k_2$ , the activity of the ubiquitin pathway, increases abruptly as [active MPF] increases. Below the cyclin balance curve we expect [total cyclin] to increase with time because the rate of cyclin synthesis is greater than cyclin degradation, and above the cyclin balance curve we expect [total cyclin] to decrease. In the same figure we also plot the dimer equilibrium curve, above which [active MPF] increases with time and below which it decreases. Thus, these two curves in the phase plane give a suggestive portrait of the state of the cell-cycle engine and its underlying dynamical forces.

The portrait is suggestive but not completely accurate because we have plotted the dimer equilibrium curve

assuming no cyclin synthesis or degradation and the cyclin balance curve assuming the degradation machinery has come to equilibrium. For this reason, the force field in Fig. 8A (the arrows) is not exactly correct. We may use the portrait to guide our intuition about the dynamics of the cell cycle engine (for example, in Fig. 8A there appears to be a spontaneous rotary motion of the state of the engine around the intersection point of the two curves), but to confirm our suspicions it is necessary to solve numerically the complete set of differential equations (Fig. 2) describing the M-phase control system.

In Fig. 8B we show that, for the parameter values given in Table 1, the cell-cycle engine does indeed exhibit sustained autonomous oscillations in MPF activity and cyclin level. (For other parameter values, the engine may halt at a stable steady state of low MPF activity (interphase arrest) or of high MPF activity (M-phase arrest), as described by Tyson (1991) and Novak and Tyson (1993).)

The oscillatory state appears as a closed orbit in the plane: the orbit is traversed in a clockwise direction once every 80 minutes. Motion around the orbit is not at constant velocity. Rather, there is a slow region, 62 minutes long, when MPF activity is small (< 0.175, indicated by the broken line), and a fast region, 18 minutes long, when MPF shows a significant peak of activity (the logarithmic scale on the MPF axis diminishes to the eye the magnitude of this peak). The peak in MPF activity we associate with M phase. In particular, we assume that, when [active MPF] increases above 0.175, nuclei in the cell or extract enter mitosis and, when it decreases below 0.175, they exit mitosis. This convention is somewhat arbitrary, but it serves well our present purposes.

We associate the oscillations in Fig. 8B with the autonomous cycles of MPF activation typically observed in *Xenopus* oocyte extracts. In Fig. 9 we plot these oscillations in a more familiar form, showing, as functions of time, the concentrations of total cyclin, active MPF, and the tyrosine-phosphorylated dimers. These time courses look similar to the original observations of Murray and Kirschner (1989) of autonomous cycles of MPF activity in *Xenopus* extracts. The changes in phosphorylation state (activity) of Wee1 and Cdc25 illustrated in Fig. 9 are consistent with observations of Solomon et al. (1990), Fig. 9; Izumi et al. (1992), Fig. 3C; Kumagai and Dunphy (1992), Fig. 4B; and Smythe and Newport (1992), Fig. 2B.

Observe that [total cyclin] rises well above 0.26 (the cyclin threshold) before MPF is activated, because there is a long lag between cyclin exceeding threshold and the positive feedback loops engaging. Because of this lag, there will be a distinct period before mitosis during which the next mitosis is independent of continued protein synthesis. This effect has been observed by Felix et al. (1989), using cycloheximide to inhibit protein synthesis, and is reproduced by our model (simulations not shown). If okadaic acid is added to post-ribosomal extracts, the next mitosis can be initiated much earlier (Felix et al., 1990a), and our model shows the same behavior (Fig. 10). Okadaic acid has this effect because it completely eliminates the cyclin threshold (Fig. 5); thus, as long as there is a sufficient quantity of preMPF, mitosis can be initiated by tryosine dephosphorylation without further protein (cyclin) synthesis.

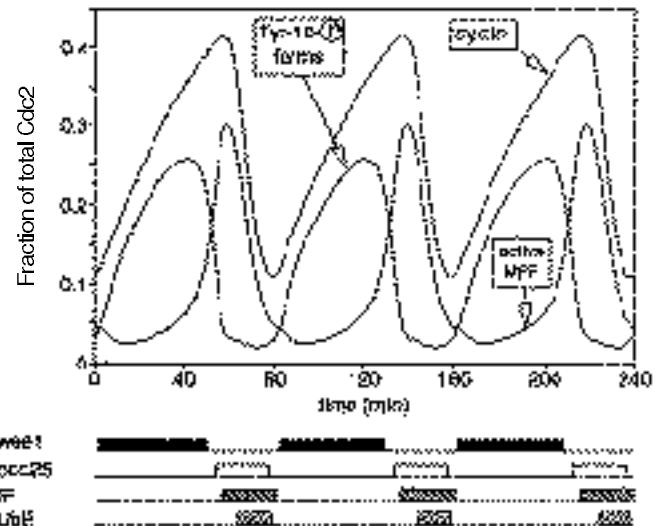


**Fig. 9.** Autonomous oscillations in the model of *Xenopus* extracts. The limit cycle in Fig. 8B is plotted here as time courses of total cyclin, active MPF and the tyrosine-phosphorylated dimers, expressed as fractions of the total amount of Cdc2. The bar graphs at the bottom indicate the periods of time during which the active forms of the indicated components exceed 50% of the total amount. Compare the top panel with Murray and Kirschner (1989), Figs 2C and 3D. Compare Wee1 with Smythe and Newport (1992), Fig. 2B.

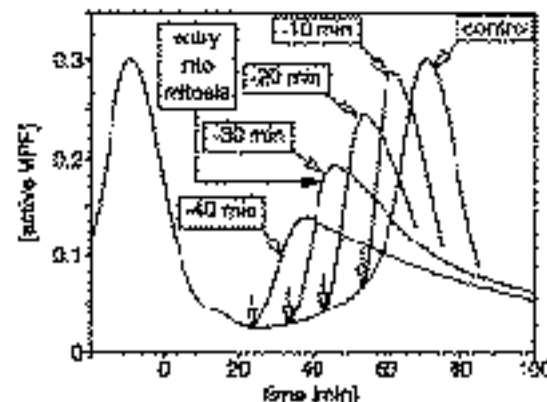


**Fig. 10.** Effect of okadaic acid on mitotic timing. Addition of okadaic acid induces premature mitosis even in the absence of further protein synthesis. In the simulations, we set  $k_1 = k_b = k_f = k_{INH} = 0$  at the indicated times. Compare with Felix et al. (1990a), Fig. 2.

Murray and Kirschner (1989) have studied the effect on cycle time of increasing the rate of cyclin synthesis by adding exogenous cyclin mRNA to *Xenopus* oocyte extracts. At 1  $\mu$ g cyclin mRNA per ml extract, the indicator nuclei could not proceed from interphase to mitosis. At 2.5  $\mu$ g/ml, the nuclei divided periodically every 60 minutes, and as they increased the cyclin mRNA level to 5  $\mu$ g/ml, the cycle time decreased to 40 minutes. To explore this effect, we calculated cycle time as a function of the rate of cyclin synthesis ( $k_1$  [AA] / [total Cdc2], or  $k_1$  for short); see Fig. 11A. For  $k_1 < 0.004 \text{ min}^{-1}$ , the control

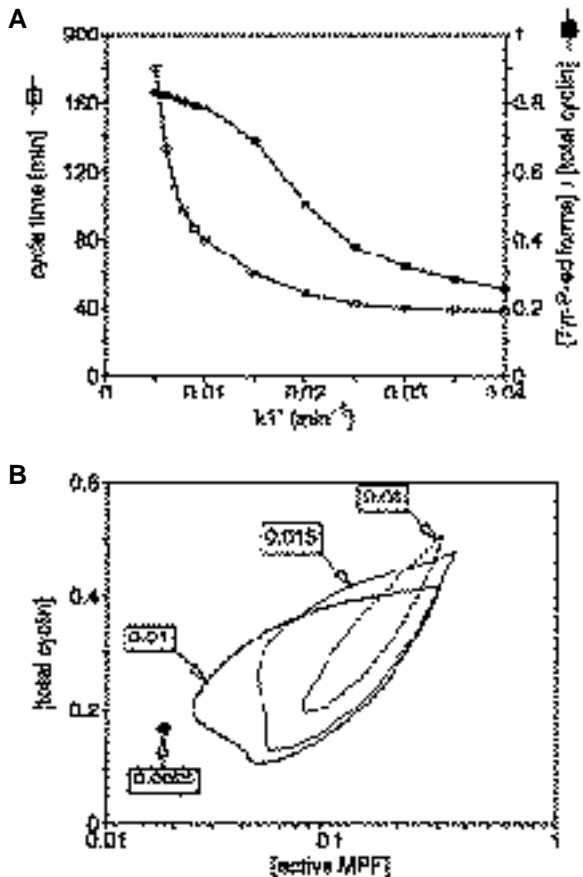
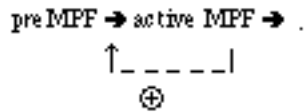


**Fig. 11.** Type  $\oplus$  and type  $\ominus$  oscillations. (A) Cycle time and the extent of tyrosine phosphorylation depend on the rate of cyclin synthesis. For  $k_1 < 0.004 \text{ min}^{-1}$ , the MPF regulatory system is stopped at a stable steady state of low MPF activity. For  $k_1 > 0.004 \text{ min}^{-1}$ , the system exhibits spontaneous oscillations whose period drops rapidly as  $k_1$  increases (open squares). We also plot (filled squares) the maximum extent of tyrosine phosphorylation during one cycle. In all cases, the minimum extent is about 8%. (B) Dynamical portraits. For  $k_1 = 0.01 \text{ min}^{-1}$ , we reproduce the limit cycle plotted in Fig. 8B. This is a type  $\oplus$  oscillation, with significant tyrosine phosphorylation during interphase, i.e. with significant involvement of the positive feedback loops through Wee1 and Cdc25. For  $k_1 = 0.03 \text{ min}^{-1}$ , the limit cycle never visits the region of state space where tyrosine is significantly phosphorylated. These are type  $\ominus$  oscillations, driven by the negative feedback loop involving cyclin degradation. For  $k_1 = 0.015 \text{ min}^{-1}$ , the oscillation is intermediate between types  $\oplus$  and  $\ominus$ . For  $k_1 = 0.0025 \text{ min}^{-1}$ , the system halts at a stable steady state (a point in state space) of low MPF activity.

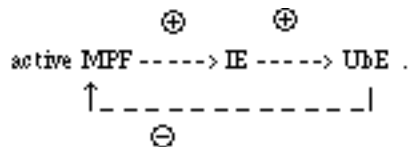
system rests at a stable steady state of low MPF activity. For  $k_1 > 0.004 \text{ min}^{-1}$ , the system oscillates with a period that drops rapidly to an asymptotic value of about 40 minutes.

At the extremes of the oscillatory range, the control system executes two very different kinds of oscillations. For  $k_1$  values just a little above  $0.004 \text{ min}^{-1}$ , we observe oscillations like those in Fig. 9: most MPF dimers are tyrosine-phosphorylated during interphase (Fig. 11A) and then converted abruptly to active MPF at the end of interphase

by triggering the positive feedback loops operating through Wee1 and Cdc25:



We call these type  $\oplus$  oscillations. This mechanism is typically operative in oocyte extracts. For larger values of  $k_1$  ( $> 0.03 \text{ min}^{-1}$ ), there is negligible phosphorylation of Tyr15 (see Fig. 11A), MPF oscillates in a higher range of activity, and the cycle time is short. These oscillations are driven by the negative feedback loop:



We call these type  $\ominus$  oscillations, and we suggest below that this mechanism is typically operative in intact embryos.

In Fig. 11 we show that the control system can be carried from type  $\oplus$  to type  $\ominus$  oscillations by increasing the rate of cyclin synthesis. In general, type  $\oplus$  oscillations are favored by rapid dimer equilibration and type  $\ominus$  oscillations by rapid cyclin synthesis and degradation. We can explain this tendency intuitively as follows. On the phase plane in Fig. 11B, the rate of motion in the horizontal direction is determined by the rate of dimer equilibration and the rate of motion in the vertical direction by cyclin turnover. At the lowest point of the oscillation, the system has to make a 'decision' either to keep moving leftward (tyrosine phosphorylation, so dimers accumulate first as preMPF as cyclin is synthesized) or to turn back to the right (tyrosine phosphatase remains active, so dimers accumulate directly as active MPF as cyclin is synthesized). As we increase the rate of cyclin synthesis relative to the rate of dimer equilibration, we favor the tendency of the system to turn back to the right, i.e. we favor the negative feedback oscillations. At  $k_1 = 0.015 \text{ min}^{-1}$  (in Fig. 11B), we see that the two tendencies are almost in balance: the system point turns neither to the left nor to the right but moves up along an oscillatory path intermediate between type  $\oplus$  and type  $\ominus$  oscillations.

The mitotic control system (Fig. 1) contains two different sources of oscillatory instability: autocatalytic activation of MPF by dephosphorylating preMPF forms, and a negative feedback loop operating through cyclin degradation. For some parameter sets the positive feedback loop is predominant, whereas for others the negative feedback loop is the major source of oscillation. The two extremes are easily recognizable, but on closer inspection one may be able to see the control system move smoothly between them as physiological conditions change (Fig. 11B). In earlier theoretical work, we have emphasized the role of MPF autocatalysis via tyrosine dephosphorylation (Tyson, 1991; Novak and Tyson, 1993), and Goldbeter (1991, 1993) has pointed to negative feedback as the source of oscillations in early embryos. But clearly both destabilizing features of the mitotic control system are important.

## MPF CYCLES IN OOCYTE EXTRACTS CONTAINING EXOGENOUS SPERM NUCLEI

The effects of DNA on MPF cycles in *Xenopus* extracts are various and illuminating. Extracts prepared with little or no DNA (i.e. with or without the maternal nucleus) exhibit spontaneous oscillations, as described in the previous section. Limited amounts of exogenous DNA (sperm nuclei) can be added without any dramatic change in MPF cycles. The DNA is replicated by the extract and the nuclei divide when MPF is activated. However, if DNA synthesis is inhibited by adding aphidicolin to the extract, then the cycle-time for MPF activation is dramatically lengthened (Dasso and Newport, 1990). Cycle time increases with increasing numbers of unreplicated sperm nuclei (Fig. 12A,

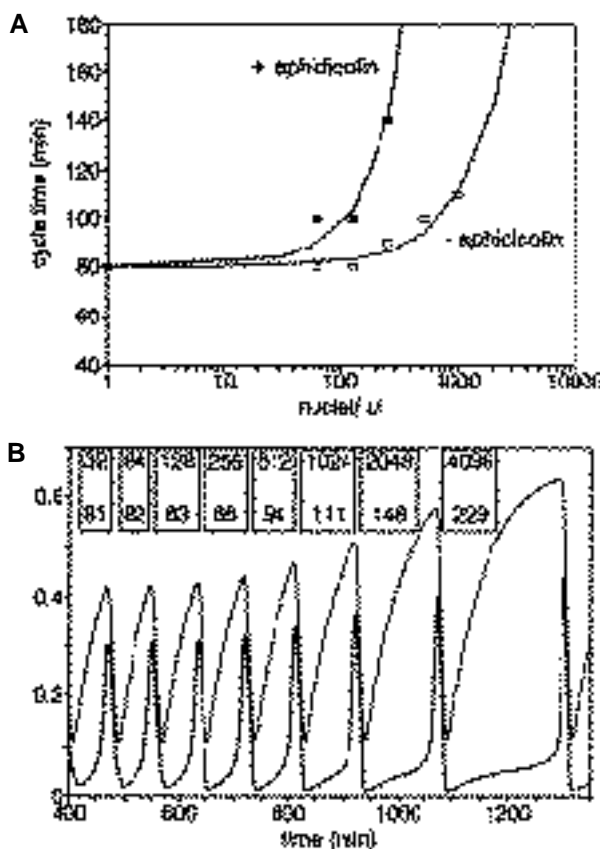


**Fig. 12.** MPF oscillations in extracts containing sperm nuclei. (A) Effect of sperm nuclei in the presence or absence of aphidicolin. Filled squares, sperm nuclei+aphidicolin; open squares, sperm nuclei without aphidicolin (data from Dasso and Newport (1990), Fig. 3, plus 20 minutes for mitosis; used by permission of John Newport). The continuous lines were calculated from the model, as described in the text. The theoretical curve through the open squares is derived from the data in (B). (B) Cycles 6-13 in an extract that is replicating DNA. We start initially with one nucleus which replicates and divides in the first cycle, etc., and we start recording at the beginning of cycle 6. In the box above each cycle we indicate the number of nuclei (top) in the extract and the cycle time (in min, below). Dotted line, total cyclin; continuous line, active MPF. Notice that the pattern of MPF activity becomes biphasic in the later cycles, exactly as observed by Dasso and Newport (1990), Fig. 4A.

filled squares), up to about 350 nuclei per  $\mu\text{l}$  extract; above this value, MPF no longer cycles and the nuclei are stuck in interphase.

In our model, unreplicated DNA prevents the activation of MPF by stimulating phosphatase f, which activates Wee1 (Smythe and Newport, 1992), and phosphatase b, which inhibits Cdc25 (Izumi et al., 1992; Walker et al., 1992). The dynamical effect of activating these phosphatases is to shift the 'switch-over point' for Wee1 and Cdc25\* to higher concentrations of active MPF (Fig. 3A). As a result, as the amount of unreplicated DNA in a cell increases, it becomes more difficult to ignite the autocatalytic loop, the local maximum of the dimer equilibrium curve shifts to higher cyclin concentration, and, above a certain threshold level of unreplicated DNA, the control system arrests with a low level of active MPF.

To extend our model to extracts containing sperm nuclei and aphidicolin, we need to specify how  $k_b$  and  $k_f$  depend on unreplicated DNA. To fit the observation of Dasso and Newport (1990) that 256 nuclei per  $\mu\text{l}$  in the presence of aphidicolin give a cycle time of 140 minutes, we assume that:

$$k_b = 0.125 + 0.1 \frac{\text{unrepDNA}}{256 \text{ nuclei}/\mu\text{l}},$$

$$k_f = 0.1 + 0.08 \frac{\text{unrepDNA}}{256 \text{ nuclei}/\mu\text{l}}.$$

By increasing  $k_b$  and  $k_f$ , unreplicated DNA causes the local maximum of the dimer equilibrium curve to increase (Fig. 5B), so the extract must synthesize progressively more cyclin to climb the hill, and this lengthens the period between MPF activity peaks (Fig. 12A, continuous line near the filled squares). Eventually, the extract contains so much unreplicated DNA ( $> 400$  nuclei/ $\mu\text{l}$ ) that the control system sticks at a stable steady state of interphase arrest. Our simulations (not shown) are consistent with Dasso and Newport's (1990) observation (their Fig. 4B) that cyclin levels off at a high plateau and Cdc2-kinase activity remains low in these aphidicolin-arrested extracts.

This steady state of interphase arrest is really an 'S-phase checkpoint.' The control system cannot proceed to M phase because the extract contains too much unreplicated DNA. However, if Cdc25 is added to an aphidicolin-blocked extract, it enters mitosis (Kumagai and Dunphy, 1991; Dasso et al., 1992). The antagonistic action of unreplicated DNA and Cdc25 is evident in Fig. 5: unreplicated DNA pushes up the cyclin threshold and additional Cdc25 pushes it down. An aphidicolin block can also be released by okadaic acid (Smythe and Newport, 1992; Izumi et al., 1992), which completely eliminates the local maximum of

\*Observe that, in interphase (when MPF activity is low), Cdc25 exists primarily in the inactive form and it can be made only slightly more inactive by adding unreplicated DNA to the extract (Fig. 3). Thus, it would appear that Cdc25 is not regulated by unreplicated DNA (Kumagai and Dunphy, 1992). However, in our model, it is not the activity of Cdc25 that is directly affected by unreplicated DNA but rather the phosphatase that opposes MPF in the phosphorylation and dephosphorylation of Cdc25. As a consequence, the level of MPF activity that is required to switch Cdc25 from its inactive to its active state increases with increasing amounts of unreplicated DNA.

the equilibrium curve (Fig. 5) and allows the inactive stores of MPF to be activated.

Since unreplicated DNA and Cdc25 have antagonistic effects on the local maximum of the dimer equilibrium curve, the threshold number of unreplicated nuclei needed to arrest the cycle should depend on Cdc25 activity. By inhibiting Cdc25 partially with increasing concentrations of vanadate, Dasso et al. (1992) found that fewer unreplicated nuclei are needed to cause interphase arrest, exactly as expected by the model.

In the absence of aphidicolin, extracts which contain lots of sperm nuclei have increasingly longer cycle times (Dasso and Newport, 1990; see their data, open squares, on our Fig. 12A). Cycle time is lengthened because S phase is extended (not because a G<sub>2</sub> phase is inserted into the cell cycle). In our model, if DNA cannot be completely replicated in the normally allotted time (while cyclin is accumulating to the threshold), then the S-phase checkpoint will arrest the MPF cycle in interphase until only 400 nuclear units of DNA per  $\mu\text{l}$  remain to be replicated. At that point the arrest is removed and the control system proceeds toward MPF activation, assured that the remaining nuclei can be replicated before chromosome condensation is initiated.

To simulate this effect, we need to know how fast DNA is synthesized in *Xenopus* extracts. From Dasso and Newport's experiments (Fig. 12A, open squares) we find that the duration of S phase ( $t_S$ ) increases linearly with the number ( $n$ ) of nuclei per  $\mu\text{l}$  extract:  $t_S = 56 \text{ min} + (n/25) \text{ min}$ . Since  $n$  nuclei are replicated during S phase, the average rate of nuclear replication is  $n/t_S$ , or:

$$v(n) = \left( 25 \frac{\text{nuclei}}{\text{min}} \right) \left( \frac{n}{1400 + n} \right).$$

This is a Michaelis-Menten-type rate law, suggesting that nuclei are competing for the replication machinery.

At the beginning of S phase,  $n$  nuclei are being replicated at an average rate  $v(n)$ . At time  $t$  into S phase:

$$\text{unrep1DNA} = n - v(n) \cdot t = n \left( 1 - \frac{25t}{1400 + n} \right).$$

Using this number, we compute values of  $k_b$  and  $k_f$  (from the equations above), and solve the differential equations in Fig. 2 with these time-dependent rate 'constants'. The results of such a simulation are shown in Fig. 12A (continuous line near the open squares) and Fig. 12B. The increase in cycle time with increasing nuclear content is due entirely to extension of S phase.

## EARLY EMBRYONIC CYCLES

Although MPF oscillations in cell-free extracts of *Xenopus* oocytes are well described by type  $\oplus$  oscillations in the model, early cell cycles (2-12) in intact frog embryos are shorter and more typical of type  $\ominus$  oscillations in that Cdc2 is not significantly tyrosine-phosphorylated (Ferrell et al., 1991). (The very first cycle is longer than the next 11, and Cdc2 is tyrosine-phosphorylated during the first interphase.)

After cycle 12 (the mid-blastula transition), cell division becomes asynchronous, and cell cycles lengthen dramatically because S phase increases in duration (Dasso and Newport, 1990) and gaps G<sub>1</sub> and G<sub>2</sub> enter the cycle.

In a previous section we saw that type  $\ominus$  oscillations arise when cyclin synthesis is fast compared to dimer equilibration. Felix et al. (1989) and Luca and Ruderman (1989) have remarked that cyclin turnover is faster in intact embryos than in oocyte extracts. In addition, large values of [total Cdc25] predispose the system to type  $\ominus$  oscillations, and early embryos seem to have copious amounts of this phosphatase (Jessus and Beach, 1992; Izumi et al., 1992). By partially inhibiting cyclin synthesis in embryos with small doses of cycloheximide, one might be able to switch cycles 2-12 from type  $\ominus$  to type  $\oplus$  oscillations.

In Fig. 13 we show a simulation of early embryonic cell cycles and the mid-blastula transition. We start the simulation at some point after fertilization with very little cyclin and the few remaining cyclin-Cdc2 dimers in the tyrosine-phosphorylated form. Thus, during the first cycle, dimers accumulate as preMPF, and mitosis 1 is triggered when [total cyclin] rises above threshold. Cycles 2-11, on the other hand, show little tyrosine phosphorylation and are of uniform short duration. During these cycles, the DNA content of the embryo is increasing exponentially. In interphase unreplicated DNA interferes with the mitotic oscillator by increasing the activities of phosphatases b and f, but this effect is negligible at first. However, very abruptly in cycle 12 there is enough unreplicated DNA to shift the control system toward tyrosine phosphorylation. When this happens, MPF remains in inactive tyrosine-phosphorylated forms until DNA replication is almost complete, and inhibition of the positive feedback loops is released. Thus, it appears in this model that the mid-blastula transition is a transition from rapid type  $\ominus$  oscillations (driven by MPF stimulating its own destruction by cyclin degradation) to slower type  $\oplus$  oscillations (driven by MPF stimulating its own activation by tyrosine dephosphorylation).

The increase in cycle time in Fig. 13 is due entirely to extension of S phase. No G<sub>2</sub> phase is inserted into the cycle as long as [total Cdc25] stays high. However, about the time of the mid-blastula transition, the maternal supply of Cdc25 starts to be depleted, becoming so low that, even after DNA is completely replicated, the cell-cycle engine remains stuck in a stable state of interphase arrest. In this case, a G<sub>2</sub> phase enters the cell cycle: some other condition besides completion of DNA synthesis must be satisfied before interphase arrest is lifted and the cell can proceed to mitosis. This other requirement seems to be synthesis of Cdc25 (Nurse, 1990). A model of slow S-G<sub>2</sub>-M cycles driven by Cdc25 accumulation is described by Novak and Tyson (1993).

## DISCUSSION

In all eukaryotic cells studied to date, mitosis is triggered by MPF, a cyclin-dependent protein kinase that is periodically activated and inactivated during the cell cycle. MPF activity is regulated by synthesis and degradation of its cyclin B subunit and by phosphorylation and dephos-

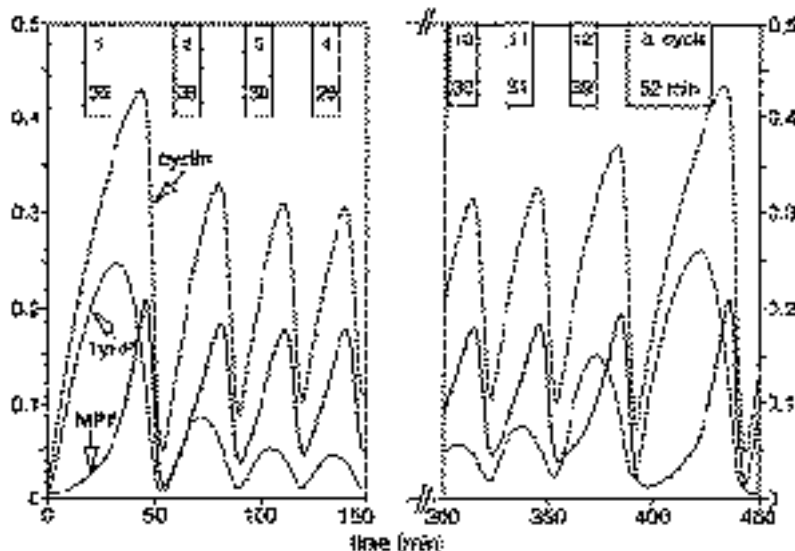


**Fig. 13.** Oscillations 1-13 in the *Xenopus* embryo. In the first cycle, Tyr15 is phosphorylated, but in cycles 2-11 only a minor fraction of Cdc2-cyclin dimers are phosphorylated. In cycle 12 the control system switches from rapid type  $\ominus$  oscillations (cycles 2-11) to slower type  $\oplus$  oscillations (cycle 13 and following). This simulation was carried out using the *alternative* parameter values in Table 1, with  $k_b$  and  $k_f$  dependent on unreplicated DNA:  $k_b=0.0375+(1.6\times 10^{-5})(\text{unrep DNA})$  and  $k_f=0.05+(2.13\times 10^{-5})(\text{unrep DNA})$ , and with the amount of unreplicated DNA given by the number  $n$  of nuclei and the time  $t$  into S phase: unrep DNA =  $n(1-(1000t/15000+n))$ . The initial conditions corresponded to low levels of total cyclin and active MPF.

phorylation of its kinase subunit (Cdc2) at an activatory threonine residue and an inhibitory tyrosine residue. From a variety of experiments on cell-free preparations of *Xenopus* oocytes, we have constructed a comprehensive model of MPF activation (Fig. 1) with two characteristic features: (1) equilibration of cyclin-Cdc2 dimers among four different phosphorylation states, influenced dramatically by positive feedback of active MPF on the tyrosine kinase and phosphatase; and (2) degradation of cyclin by a ubiquitin pathway that is activated indirectly by MPF. The model presents a unified, coherent, and testable picture of M-phase control in *Xenopus* oocytes and embryos.

When examining any small piece of this system, cell biologists can usually rely on their intuitive understanding of molecular interactions to predict qualitative changes in response to experimental manipulation; but when we put together a reasonably complete picture of the regulation of MPF activity and address to it quantitative questions about timing and extent, casual verbal arguments are insufficient and we must turn to the precise language of mathematics (Maddox, 1992). In this paper, we illustrate how a theoretical approach can be applied to M-phase control by translating the reaction network (Fig. 1) into a set of differential equations (Fig. 2) that describe the time-dependent changes in concentrations of the major components of the control system, and by solving these equations by accurate numerical methods.

Using this approach we have compared our model in quantitative detail with several types of experiments on *Xenopus* oocyte extracts: (1) cyclin-induced activation of MPF (Fig. 4); (2) MPF-induced activation of MPF (Fig. 6); (3) MPF-induced degradation of cyclin (Fig. 7); (4) autonomous oscillations in MPF activity and cyclin level (Fig. 9); (5) inhibition of oscillations by unreplicated DNA (Fig. 12); and with autonomous oscillations in intact embryos (Fig. 13).

Although the comparison between model and observation is made by numerical solution of the underlying differential equations, a numerical approach alone is not very satisfying. Looking at computer output from a complicated set of differential equations is less illuminating than look-

ing at experimental output from the intact organism. To try to understand the inner workings of the cell-cycle engine, we have introduced an approximate graphical approach to the problem. Of the nine variables that describe the complete state of our model, we keep track of the two most important ones: total cyclin and active MPF. Letting the vertical axis of a coordinate system represent [total cyclin] and the horizontal axis [active MPF], we can represent the instantaneous state of the control system as a point in this plane (called the phase plane). To reveal the dynamics of the system, we plot on this coordinate system two characteristic curves: the dimer equilibrium curve and the cyclin balance curve. These two curves tell us the direction in which the control system evolves as the underlying chemical reactions drive changes in cyclin level and MPF activity. A picture of the dimer equilibrium and cyclin balance curves in the phase plane is called a ‘dynamical portrait’ of the model (e.g. Fig. 8). As physiological conditions of the cell or extract change, the parameters of the control system change, and the dynamical portrait also changes (Tyson, 1991). We use these changes in dimer equilibrium and cyclin balance curves to guide our investigations of the cell-cycle engine.

The dimer equilibrium curve is **N**-shaped (Fig. 3B) as a consequence of the sigmoidal dependence of the regulatory enzymes (Wee1 and Cdc25) on MPF activity (Fig. 3A). The **N** shape implies that there must be a threshold for cyclin-induced activation of MPF: it is just the local maximum of the dimer equilibrium curve (Fig. 4B). The height of this maximum can be changed in predictable ways by treatments that interfere with the regulation of Wee1 and Cdc25 activities; such as supplementing an extract with more Cdc25 or INH, or adding phosphatase inhibitors (Fig. 5). The **N** shape also implies that, for a fixed cyclin level below threshold, there must be an MPF threshold for MPF activation: it is roughly the distance across the ‘barrier’ at the fixed cyclin level (the distance between points 1 and 3 in Fig. 3B). Clearly the two thresholds are related: any treatment that increases the cyclin threshold will also increase the MPF threshold.

Following Izumi et al. (1992) and Dasso et al. (1992),

we assume that unreplicated DNA in a cell increases the activities of the enzymes that dephosphorylate Cdc25 and Wee1, and consequently raises the local maximum of the dimer equilibrium curve (Fig. 5). This effect allows unreplicated DNA to serve as a checkpoint signal to arrest (or at least slow down) the cell cycle until DNA replication is complete. There is, therefore, in *Xenopus* eggs and extracts, a third threshold: the minimum level of unreplicated DNA necessary to block progress toward mitosis. All three thresholds are related to the local maximum of the dimer equilibrium curve, which is generated by the positive feedback loops operating through Wee1 and Cdc25.

Our model exhibits two types of oscillations: type  $\oplus$ , driven by periodic tyrosine phosphorylation and typical of oocyte extracts (Fig. 9); and type  $\ominus$ , driven by the negative feedback loop of MPF on its own destruction and typical of early embryonic cell cycles (Fig. 13). Which type of oscillation the control system executes depends on the rate of cyclin synthesis relative to the rate of tyrosine phosphorylation of MPF dimers (Fig. 11).

Compared to oocyte extracts, intact frog embryos seem to have more rapid cyclin turnover (Felix et al., 1989; Luca and Ruderman, 1989), which favors type  $\ominus$  oscillations: Cdc25 remains active and Wee1 inactive, but the system cannot come to rest at a steady state of high MPF activity because the negative feedback loop renders that state unstable. The system executes rapid type  $\ominus$  oscillations as it switches back and forth between phases of net cyclin synthesis and degradation. Although MPF activity fluctuates concomitantly, it is always large enough to keep the positive feedback loop almost fully engaged and Tyr15 mostly unphosphorylated. Active MPF accumulates as cyclin is synthesized, and it initiates cyclin degradation on passing a certain threshold. But the lag time in the ubiquitin pathway permits active MPF to overshoot the threshold before it is removed by cyclin degradation. Successive overshoots and undershoots, caused by the time lag, prevent the control system from settling on a steady state where cyclin synthesis and degradation are balanced.

On the other hand, if conditions change to favor active Wee1 and inactive Cdc25 (e.g. in the presence of unreplicated DNA), then the control system can bring the positive feedback loop into play. When this loop switches to the on position, Tyr15 becomes phosphorylated and Cdc2-cyclin dimers accumulate as inactive preMPF. The cell or extract must synthesize enough cyclin to surmount the threshold for cyclin-induced dephosphorylation of Tyr15. If the rate of cyclin synthesis relative to degradation is too small, cyclin may never rise above threshold. In this case, the control system arrests in a state of low MPF activity.

The arrested state can serve as a checkpoint in the cell cycle. Somatic cells are arrested here until certain conditions are met: is DNA replication complete? Is the cell sufficiently large? These conditions must be fulfilled in order to destabilize the steady state and allow the positive feedback loop to convert preMPF to active MPF. In embryonic cells, on the other hand, these checkpoint controls may not be fully operative (Enoch and Nurse, 1991) because an excess of Cdc25 pushes down the dimer equilibrium curve thereby attenuating or removing the interphase checkpoint.

Our model is open to experimental tests on many fronts. For instance:

(1) The N-shaped dimer equilibrium curve predicts not only a cyclin threshold for MPF activation but also a cyclin threshold for MPF inactivation. Between the two thresholds there is a region of alternative stable states of dimer equilibrium with MPF activity either large or small.

(2) The lag time for cyclin-induced MPF activation should increase dramatically as cyclin approaches the threshold level from above. This effect has not been described in the literature.

(3) By adding increasing amounts of cyclin mRNA to oocyte extracts ablated of endogenous message, one should be able to carry the control system continuously from type  $\oplus$  to type  $\ominus$  oscillations.

Experiments like these would confirm or refute the dynamical feedback loops on which our model is built.

We have tried to present and analyze a model of M-phase control in *Xenopus* eggs and extracts that is reasonably complete and believable. We have compared the behavior of the model to a host of experiments in both oocyte extracts and intact embryos, and the fit of theory to experiment is gratifyingly close. Although the model is quite successful as it stands, it is certain to change as new information appears regarding M-phase control in *Xenopus* cells, as the model is applied to different organisms, and as more is learned about S-phase control and S-M coupling. But, as our understanding of the molecular mechanism of cell cycle control in eukaryotic cells becomes more complete and more complicated, the need for realistic mathematical models of the type explored here will become ever more acute.

We acknowledge support from NSF grants DMS-9123674, MCB-9207160, and INT-9212471, from the Research Division of Virginia Tech, and from the Hungarian Academy of Science, grant OTKA 5-376. We have benefitted greatly from discussions of this problem with Mark Solomon, James Maller, Eric Karsenti and Tim Hunt. Some of our ideas about negative feedback oscillations in intact embryos we owe to Garry Odell. Thanks also to Kathy Chen for constantly and carefully critiquing our ideas.

## REFERENCES

- Clarke, P. R., Hoffmann, I., Draetta, G. and Karsenti, E. (1993). Dephosphorylation of cdc25-C by a type-2A protein phosphatase: Specific regulation during the cell cycle in *Xenopus* egg extracts. *Mol. Biol. Cell* **4**, 397-411.
- Clarke, P. R. and Karsenti, E. (1991). Regulation of p34<sup>cdc2</sup> protein kinase: new insights into protein phosphorylation and the cell cycle. *J. Cell Sci.* **100**, 409-414.
- Clarke, P. R., Leiss, D., Pagano, M. and Karsenti, E. (1992). Cyclin A- and cyclin B-dependent protein kinases are regulated by different mechanisms in *Xenopus* egg extracts. *EMBO J.* **11**, 1751-1761.
- Coleman, T. R., Tang, Z. and Dunphy, W. G. (1993). Negative regulation of the Wee1 protein kinase by direct action of the Nim1/Cdr1 mitotic inducer. *Cell* **72**, 919-929.
- Cyert, M. S. and Kirschner, M. W. (1988). Regulation of MPF activity in vitro. *Cell* **53**, 185-195.
- Dasso, M. and Newport, J. W. (1990). Completion of DNA replication is monitored by a feedback system that controls the initiation of mitosis in vitro: studies in *Xenopus*. *Cell* **61**, 811-823.
- Dasso, M., Smythe, C., Milarski, K., Kornbluth, S. and Newport, J. W. (1992). DNA replication and progression through the cell cycle. In

- Regulation of the Eukaryotic Cell Cycle*, pp. 161-180. Chichester: John Wiley & Sons.
- Devault, A., Fesquet, D., Cavadore, J.-C., Garrigues, A.-M., Labbe, J.-C., Lorca, T., Picard, A., Philippe, M. and Doree, M.** (1992). Cyclin A potentiates maturation-promoting factor activation in the early Xenopus embryo via inhibition of the tyrosine kinase that phosphorylates cdc2. *J. Cell Biol.* **118**, 1109-1120.
- Dunphy, W. G. and Newport, J. W.** (1988). Mitosis-inducing factors are present in a latent form during interphase in the Xenopus embryo. *J. Cell Biol.* **106**, 2047-2056.
- Enoch, T. and Nurse, P.** (1991). Coupling M phase and S phase: controls maintaining the dependence of mitosis on chromosome replication. *Cell* **65**, 921-923.
- Ermentrout, B.** (1990). *Phase Plane: The Dynamical Systems Tool, Version 3.0*. Pacific Grove, CA: Brooks/Cole.
- Felix, M.-A., Cohen, P. and Karsenti, E.** (1990a). cdc2 H1 kinase is negatively regulated by a type 2A phosphatase in the Xenopus early embryonic cell cycle: evidence from the effects of okadaic acid. *EMBO J.* **9**, 675-683.
- Felix, M.-A., Labbe, J.-C., Doree, M., Hunt, T. and Karsenti, E.** (1990b). Triggering of cyclin degradation in interphase extracts of amphibian eggs by cdc2 kinase. *Nature* **346**, 379-382.
- Felix, M.-A., Pines, J., Hunt, T. and Karsenti, E.** (1989). A post-ribosomal supernatant from activated Xenopus eggs that displays post-translationally regulated oscillation of its cdc2<sup>+</sup> mitotic kinase activity. *EMBO J.* **8**, 3059-3069.
- Farrell, J. E. Jr, Wu, M., Gerhardt, J. C. and Martin, G. S.** (1991). Cell cycle tyrosine phosphorylation of p34<sup>cdc2</sup> and a microtubule-associated protein kinase homolog in Xenopus oocytes and eggs. *Mol. Cell. Biol.* **11**, 1965-1971.
- Gautier, J., Solomon, M. J., Booher, R. N., Bazan, J. F. and Kirschner, M. W.** (1991). cdc25 is a specific tyrosine phosphatase that directly activates p34<sup>cdc2</sup>. *Cell* **67**, 197-211.
- Gerhart, J., Wu, M. and Kirschner, M.** (1984). Cell cycle dynamics of an M-phase-specific cytoplasmic factor in Xenopus laevis oocytes and eggs. *J. Cell Biol.* **98**, 1247-1255.
- Glotzer, M., Murray, A. W. and Kirschner, M. W.** (1991). Cyclin is degraded by the ubiquitin pathway. *Nature* **349**, 132-138.
- Goldbeter, A.** (1991). A minimal cascade model for the mitotic oscillator involving cyclin and cdc2 kinase. *Proc. Nat. Acad. Sci. USA* **88**, 9107-9111.
- Goldbeter, A.** (1993). Modeling the mitotic oscillator driving the cell division cycle. *Comm. Theor. Biol.* (in press).
- Goldbeter, A. and Koshland, D. E. Jr** (1981). An amplified sensitivity arising from covalent modification in biological systems. *Proc. Nat. Acad. Sci. USA* **78**, 6840-6844.
- Hara, K., Tydeman, P. and Kirschner, M.** (1980). A cytoplasmic clock with the same period as the division cycle in Xenopus eggs. *Proc. Nat. Acad. Sci. USA* **77**, 462-466.
- Harvey, E. B.** (1940). A comparison of the development of nucleate and non-nucleate eggs of *Arbacia punctulata*. *Biol. Bull. Mar. Biol. Labs. Woods Hole* **79**, 166-187.
- Hoffmann, I., Clarke, P. R., Marcote, M. J., Karsenti, E. and Draetta, G.** (1993). Phosphorylation and activation of human cdc25-C by cdc2-cyclin B and its involvement in the self-amplification of MPF at mitosis. *EMBO J.* **12**, 53-63.
- Hunt, T.** (1991). Destruction's our delight. *Nature* **349**, 100-101.
- Hutchison, C. J., Cox, R. and Ford, C. C.** (1988). The control of DNA replication in a cell-free extract that recapitulates a basic cell cycle in vitro. *Development* **103**, 553-566.
- Izumi, T., Walker, D. H. and Maller, J. L.** (1992). Periodic changes in phosphorylation of the Xenopus cdc25 phosphatase regulate its activity. *Mol. Biol. Cell* **3**, 927-939.
- Jesus, C. and Beach, D.** (1992). Oscillation of MPF is accompanied by periodic association between cdc25 and cdc2-cyclin B. *Cell* **68**, 323-332.
- Kirchner, T. B.** (1990). *Time-Zero: The Integrated Modeling Environment, Version 2*. Fort Collins, CO: Quaternary Software.
- Kumagai, A. and Dunphy, W. G.** (1991). The cdc25 protein controls tyrosine dephosphorylation of the cdc2 protein in a cell-free system. *Cell* **64**, 903-914.
- Kumagai, A. and Dunphy, W. G.** (1992). Regulation of the cdc25 protein during the cell cycle in Xenopus extracts. *Cell* **70**, 139-151.
- Lorca, T., Labbe, J.-C., Devault, A., Fesquet, D., Capony, J.-P., Cavadore, J.-C., Le Bouffant, F. and Doree, M.** (1992). Dephosphorylation of cdc2 on threonine 161 is required for cdc2 kinase inactivation and normal anaphase. *EMBO J.* **11**, 2381-2390.
- Luca, F. C. and Ruderman, J. V.** (1989). Control of programmed cyclin destruction in a cell-free system. *J. Cell Biol.* **109**, 1895-1909.
- Maddox, J.** (1992). Is molecular biology yet a science? *Nature* **355**, 201.
- Maller, J. L.** (1991). Mitotic control. *Curr. Opin. Cell Biol.* **3**, 269-275.
- Masui, Y. and Markert, C. L.** (1971). Cytoplasmic control of nuclear behavior during meiotic maturation of frog oocytes. *J. Exp. Zool.* **177**, 129-146.
- Miake-Lye, R., Newport, J. and Kirschner, M.** (1983). Maturation-promoting factor induces nuclear envelope breakdown in cycloheximide-arrested embryos of Xenopus laevis. *J. Cell Biol.* **97**, 81-91.
- Murray, A. W.** (1992). Creative blocks: cell-cycle checkpoints and feedback controls. *Nature* **359**, 599-604.
- Murray, A. W.** (1993). Turning on mitosis. *Curr. Biol.* **3**, 291-293.
- Murray, A. W. and Kirschner, M. W.** (1989). Cyclin synthesis drives the early embryonic cell cycle. *Nature* **339**, 275-280.
- Murray, A. W., Solomon, M. J. and Kirschner, M. W.** (1989). The role of cyclin synthesis and degradation in the control of maturation promoting factor activity. *Nature* **339**, 280-286.
- Novak, B. and Tyson, J. J.** (1993). Modeling the cell division cycle: M-phase trigger, oscillations and size control. *J. Theor. Biol.* (in press).
- Nurse, P.** (1990). Universal control mechanism regulating onset of M-phase. *Nature* **344**, 503-508.
- Smythe, C. and Newport, J. W.** (1992). Coupling of mitosis to the completion of S phase in Xenopus occurs via modulation of the tyrosine kinase that phosphorylates p34<sup>cdc2</sup>. *Cell* **68**, 787-797.
- Solomon, M. J.** (1993). Activation of the various cyclin/cdc2 protein kinases. *Curr. Opin. Cell Biol.* **5**, 180-186.
- Solomon, M. J., Glotzer, M., Lee, T. H., Philippe, M. and Kirschner, M. W.** (1990). Cyclin activation of p34<sup>cdc2</sup>. *Cell* **63**, 1013-1024.
- Solomon, M. J., Lee, T. and Kirschner, M. W.** (1992). Role of phosphorylation in p34<sup>cdc2</sup> activation: identification of an activating kinase. *Mol. Biol.* **3**, 13-27.
- Tyson, J. J.** (1991). Modeling the cell division cycle: cdc2 and cyclin interactions. *Proc. Nat. Acad. Sci. USA* **88**, 7328-7332.
- Walker, D. H., DePaoli-Roach, A. A. and Maller, J. L.** (1992). Multiple roles for protein phosphatase 1 in regulating the Xenopus early embryonic cell cycle. *Mol. Biol. Cell* **3**, 687-698.
- Wu, M. and Gerhart, J. C.** (1980). Partial purification and characterization of the maturation-promoting factor from eggs of *Xenopus laevis*. *Dev. Biol.* **79**, 465-477.

(Received 8 June 1993 - Accepted 25 August 1993)